

Coupled air–mixed-layer temperature predictability for climate reconstruction

ANGELINE G. PENDERGRASS * GREGORY J. HAKIM, DAVID S. BATTISTI

University of Washington, Department of Atmospheric Sciences, Seattle, WA, USA

GERARD ROE

University of Washington, Department of Earth and Space Sciences, Seattle, WA, USA

* *Corresponding author address:* Angeline G. Pendergrass, University of Washington, Department of Atmospheric Sciences, Box 351640, Seattle, WA 98195.

E-mail: angie@atmos.washington.edu

ABSTRACT

A central issue for understanding past climates involves the use of sparse time-integrated data to recover the physical properties of the coupled climate system. We explore this issue in a simple model of the midlatitude climate system that has attributes consistent with the observed climate. A quasigeostrophic (QG) model thermally coupled to a slab ocean is used to approximate midlatitude coupled variability, and a variant of the ensemble Kalman filter is used to assimilate time-averaged observations. Dependence of reconstruction skill on coupling and thermal inertia are explored. Results from this model are compared with those for an even simpler two-variable linear stochastic model of midlatitude air–sea interaction, for which the assimilation problem can be solved semi-analytically.

Results for the QG model show that skill decreases as averaging time increases in both the atmosphere and ocean when normalized against the time-averaged climatological variance. Skill in the ocean increases with slab depth, as expected from thermal-inertia arguments, but skill in the atmosphere decreases. An explanation of this counterintuitive result derives from an analytical expression for the forecast error covariance in the two-variable stochastic model, which shows that the relative fraction of noise to total error increases with slab-ocean depth. Essentially, noise becomes trapped in the atmosphere by a thermally stiffer ocean, which dominates the decrease in initial-condition error due to improved skill on the ocean.

Increasing coupling strength in the QG model yields higher skill in the atmosphere and lower skill in the ocean, as the atmosphere accesses the longer ocean memory and the ocean accesses more atmospheric high-frequency “noise.” The two-variable stochastic model fails to capture this effect, showing decreasing skill in both the atmosphere and ocean for increased coupling strength, due to an increase in the relative fraction of noise to the forecast error vari-

ance. Implications for the potential for data assimilation to improve climate reconstructions are discussed.

1. Introduction

Determining the state of the climate prior to the 20th century necessarily involves paleoclimate proxy data. These data may be viewed as a relatively sparse network of noisy observations that, in many cases, are indirect records of the climate mediated by biological or chemical processes. As a result, reconstructions of past climates have relied on statistical relationships between these proxies and large-scale patterns of atmospheric variability (e.g., Mann et al. 1999). One path to potentially improving upon these statistical reconstructions involves the introduction of a dynamical model to provide independent estimates of the observations. This approach, which we refer to as dynamical climate reconstruction, links the paleoclimate reconstruction problem to weather forecasting and modern reanalysis through the theory of state estimation. Practical realizations of dynamical climate reconstruction face numerous challenges, only one of which is taken up here. We address the problem of estimating the state of coupled atmosphere-ocean climate models subject to observations involving long averaging times typical of paleo-proxy data.

One key issue for dynamical climate reconstruction concerns the predictability time horizon of the model; that is, the time for which initial-condition errors approach the climatological distribution. When the (model) predicted observations are indistinguishable from a random draw from the climatological distribution, the main value of using the model is lost. The predictability timescale needed for reconstruction is set by the proxy data, which

span a wide range of timescales. “High frequency” paleoclimate records provide information with at best seasonal, but more typically annual, resolution (e.g., Jones et al. 2009). Since atmospheric predictability is on the order of two weeks, predictability on the timescales of these paleoclimate data require dynamics coupled to “slower” parts of the climate system. For example, sea-surface temperatures have been shown to persist on interannual timescales in observations (Frankignoul and Hasselmann 1977; Davis 1976, see Deser et al. 2003 for a modern update) and models (Saravanan et al. 2000). Interest in this persistence has led to research on variability and predictability in highly idealized models for air-sea interaction (e.g., Barsugli and Battisti 1998; Saravanan and McWilliams 1998; Scott 2003). On longer timescales, there is evidence that the overturning circulation in the deep ocean couples to the atmosphere (e.g., Meehl et al. 2009), which appears responsible for predictable atmospheric signals beyond the seasonal timescale (Latif 1998; Griffies and Bryan 1997; Grotzner et al. 1999; Boer 2000; Saravanan et al. 2000; Collins 2002; Pohlmann et al. 2004; Latif et al. 2006; Boer and Lambert 2008; Koenigk and Mikolajewicz 2009).

Paleoclimate proxy data for air temperature and precipitation in midlatitudes represents climate states integrated over all of the weather during the course of a season or annual cycle. The characteristics of weather events, and the frequency with which they visit particular locations, depends on larger-scale, slower varying properties of the atmosphere and ocean. For example, extratropical cyclones organize in storm tracks, which in turn follow the location of the jet stream. Thus the reconstruction problem is one where the details of individual high-frequency features responsible for the proxy data are unknown, but the time average of these features provides information on slower components of the system.

To address this problem, we use two idealized models of a thermally coupled midlatitude

atmosphere and ocean mixed layer that represent both the relevant fast and slow dynamics. The zero-dimensional energy balance model (referred to hereafter as the BB model) was designed as an analog to the midlatitude atmosphere-ocean system by Barsugli and Battisti (1998). The quasigeostrophic (QG) model, developed by Hakim (2000), explicitly calculates the dominant atmospheric dynamics, and the slab ocean parameters were chosen to correspond to those in the BB model. So, while the models are idealized, they capture important mechanisms for paleo proxy data.

In order to exploit seasonal or longer predictive timescales and dynamically reconstruct past climate states, an estimation method is needed to identify accurate initial conditions. Here we will employ an ensemble Kalman filter (EnKF) technique applied to the above models of coupled atmosphere-ocean interaction to address two hypotheses: background climate reconstruction errors become smaller when (1) the thermal heat capacity of the ocean increases, and (2) the coupling between the ocean and atmosphere strengthens. The EnKF is particularly attractive for addressing these hypotheses because it relaxes the assumption of stationary statistics made in purely statistical reconstructions. Therefore, information about the slow component of the system (the ocean) can affect the atmosphere through both the forecast and the assimilation. Idealized models provide clean control of the processes of interest, inexpensive repeatable solutions, and results that can be tested with more complicated models.

The layout of the paper is as follows. Section 2 introduces the two models and the assimilation systems built around them. The QG model is described in section 2a, and the BB model is described in section 2b. Results are given in section 3, with those determined numerically for the QG model in section 3a and those obtained semi-analytically for the

energy-balance model in section 3b. Portions of the error for the energy balance model due to the initial conditions and accumulation of noise are described in section 3c. Conclusions are provided in section 4.

2. Method

a. Quasigeostrophic atmosphere model coupled to a slab ocean

To good approximation, the QG equations capture the dynamics of the midlatitude storm tracks. Moreover, since potential vorticity (PV) is well mixed in the troposphere, the dynamics may be further approximated by a uniform layer of PV bounded by rigid surfaces representing the surface and tropopause; this reduces the calculation in three dimensions to a two-dimensional boundary-value problem (Hakim 2000). This model, when coupled to a slab ocean model, is referred to hereafter as the QG model.

The atmosphere component of the model is a two-surface dry QG model on an f -plane that is thermally relaxed to a specified jet (Hoskins and West 1979) on a timescale of 8.6 days. The model is periodic in y and x (latitude and longitude), has an Ekman layer at the bottom boundary, and solves exactly for the full three-dimensional fields of temperature and wind given the surface potential temperature. The model was originally described in Hakim (2000) who provides additional details on the solution methods. An uncoupled version of the atmosphere model was used by Huntley and Hakim (2009) to explore the time-averaged data assimilation algorithm for paleoclimate reconstruction proposed by Dirren and Hakim (2005). Huntley and Hakim (2009) found a predictability horizon beyond which the model no

longer provided information distinct from climatology (i.e., a fixed error covariance matrix). However, this model lacked coupling to components of the climate system that have slower timescales, which we address here by thermally coupling the QG atmosphere to a slab ocean.

The slab ocean does not move and only exchanges heat with the atmosphere. In order to preserve the uniform-PV assumption of the atmosphere component of the QG model, heat is exchanged uniformly at the surface and tropopause (i.e., through the entire depth of the atmosphere), which is essentially an equivalent barotropic forcing of the atmosphere. The heat flux is determined by the temperature anomaly difference between the atmosphere’s surface and the slab ocean, modulated by a coupling constant. More realistic coupling coefficients would also involve the wind speed magnitude or its square, but these were sacrificed here for simplicity and to provide a link to the analytical model described below. Control values for the constants in the model are listed in Table 1.

This simple model provides a framework for addressing the two hypotheses in terms of two parameters: the coupling constant, and the depth of the slab ocean. While this coupled model provides a testbed to study how the atmosphere, modulated by the slow thermal inertia of a slab ocean, may be reconstructed on long time scales, it should be clear that this model does not include nonlinear aspects of heat-flux exchange (e.g., due to wind speed), ocean dynamics, changes in the mixed layer and its heat capacity, the seasonal cycle, or any precipitation–evaporation-related processes. However, it does capture the dynamics of heat exchange between a rapidly evolving atmosphere and a mixed layer with greater thermal inertia, which is fundamental in midlatitudes. We proceed now to describe the assimilation system used to reconstruct the model state from noisy observations of time-averages of the atmosphere and ocean temperature.

The EnKF data assimilation system for the QG model is implemented in the Jamaica release of the Data Assimilation Research Testbed (DART, Anderson et al. 2009), a community-oriented ensemble data assimilation system. The Ensemble Adjustment Kalman Filter (Anderson 2001) is used without covariance inflation and with covariance “localization” using the Gaspari–Cohn function (Gaspari and Cohn 1999) with a half-width of half the domain to deal with sampling error. Observations are placed at every other grid point, each with an error of 1/10 of the domain-mean climatological variance for the averaging time of the observations. Ensembles of 48 members are initialized with random draws of instantaneous states from a 2500-day integration of the model. Each experiment consists of one ensemble integration of 100 days without assimilation (the control case) and another integration with assimilation.

In order to investigate the limit of utility of the reconstruction method, we examine the background ensemble error variance, which is the error variance at the end of a forecast cycle immediately before new observations are incorporated in the assimilation cycle. For comparison, we use an ensemble integrated without assimilating any observations; so the metric for skill is the error of the background ensemble normalized by the error of the control ensemble. If this fraction is less than one, then useful information remains from the previously assimilated observations at assimilation time.

b. Stochastic energy-balance model

A simpler zero-dimensional model of the atmosphere-ocean system provides insights into the results of the more complex system described above. The model was first introduced by

Barsugli and Battisti (1998), and will be referred to hereafter as the BB model. The model utilizes the large timescale separation in the variance of the atmosphere and ocean to parameterize atmospheric nonlinearity as a stochastic process. Stochastic climate models such as the BB model have a long history of providing a null hypothesis for problems in climate dynamics, dating from Hasselmann (1976), who used a stochastic climate model to explore how persistent, large-scale sea-surface temperature anomalies could arise in midlatitude oceans.

The BB model has thermal exchange between an atmosphere and ocean, damping, and random forcing applied to the atmosphere:

$$\frac{dT_a}{dt} = c(T_o - T_a) - \tau T_a + (b - 1)T_o + N \quad (1)$$

$$d\frac{dT_o}{dt} = -c(T_o - T_a) - \tau T_o, \quad (2)$$

where T_a is the air temperature, T_o is the mixed layer temperature, d is the ratio of heat capacities between the atmosphere and mixed layer, c is the coupling strength, τ is the radiative damping timescale, b is a constant controlling the deterministic portion of the atmospheric forcing, and N is the white-noise forcing. Equations (1) and (2) can be written compactly as

$$\frac{d\vec{T}}{dt} = \mathbf{A}\vec{T} + \mathbf{N}\vec{W}, \quad (3)$$

where

$$\mathbf{A} = \begin{bmatrix} -c - \tau & c + b - 1 \\ c/d & (-c - \tau)/d \end{bmatrix}, \quad \mathbf{N} = \begin{bmatrix} N & 0 \\ 0 & 0 \end{bmatrix},$$

$\vec{T} = [T_a \ T_o]$ is a vector of the temperatures, and $\vec{W} = [W \ 0]$ is a Gaussian white-noise process. The constants b , c , d , τ , and N are chosen to be representative of climate-scale

atmosphere-ocean interaction in the midlatitudes (see Table 1 and Barsugli and Battisti 1998).

In the absence of noise forcing, this system supports two normal-mode solutions that are damped in time, which provide a convenient basis for understanding the system dynamics with noise. The first mode damps quickly, with an e -folding timescale of 3 days for the parameters in Table 1, and consists of a mainly atmospheric temperature anomaly with a weaker ocean temperature anomaly of opposite sign, as noted by Schopf (1985) for a similar deterministic model. The second mode has an e -folding timescale of 89 days, and consists of ocean and atmosphere temperature anomalies of the same sign, with larger magnitude in the ocean by roughly a factor of two. This second mode contains the “memory” in the system, which arises because the ocean anomaly is large and of the same sign as the atmosphere, so that heat exchange is minimized between the two, resulting in a slow decay.

Because the BB model contains only two variables, the data assimilation reconstruction problem can be solved semi-analytically. Since we are interested in errors, we need only solve for the error covariance matrix. The expected error covariance over infinite experiments, derived in the appendix, is:

$$\begin{aligned} \langle \bar{\varepsilon}^* \bar{\varepsilon}^{*T} \rangle &= \frac{1}{L^2} \int_0^L e^{At} \varepsilon^*(0) dt \left(\int_0^L e^{At} \varepsilon^*(0) dt \right)^T \\ &\quad + \frac{1}{L^2} \int_0^L \left(\int_s^L e^{A(t-s)} \mathbf{N} dt \right) \left(\int_s^L e^{A(t-s)} \mathbf{N} dt \right)^T ds, \end{aligned} \quad (4)$$

where ε^* is the instantaneous error of an ensemble member, $\bar{\varepsilon}^*$ is the time-averaged error of an ensemble member, L is the averaging time, \mathbf{A} is the matrix of model parameters, and \mathbf{N} is the matrix of noise forcing coefficients. The first term represents the evolution of the

initial error covariance, which for this damped system leads to a decay of error covariance. The second term involves an integral over the noise which gives exponential growth of error covariance. We will refer to this second effect as the “accumulation” of noise.

3. Results

Before presenting results, we review the hypotheses outlined in section 1. The first is that errors in climate reconstruction will be smaller when the thermal heat capacity of the ocean is larger. The crux of this idea is that increasing the thermal heat capacity lengthens the persistence timescale of anomalies in the ocean, as discussed in section 2b, which increases the information carried forward by the model to the time of the analysis. The second hypothesis is that stronger coupling between the atmosphere and ocean should also reduce errors in climate reconstruction, especially for the atmosphere. Again, since the ocean is the source of memory, stronger coupling should imprint that memory onto the atmosphere, enhancing predictability. For the ocean, the role of coupling is less clear. Stronger coupling imparts more high-frequency atmospheric “noise” into the ocean, reducing predictability, but some of the ocean’s persistence is imparted to the atmosphere, which may mitigate this effect.

The data assimilation algorithm used here is designed for dealing with paleoclimate proxy data, which averages or integrates the climate signal over a period of time. Because interpreting the effect of different averaging times is not as straightforward as instantaneous observations, we consider first the role of averaging time on the error. For instantaneous data assimilation, analysis errors should be inversely proportional to observation frequency, since, all other things being equal, more frequent observations provide more information

about the instantaneous state of the system if the model forecast is well within the predictability time horizon. For time-averaged data assimilation, the climatological variance of the states also decreases with averaging time. Therefore, we scale the observation error with climatological variance for the timescale of the observations to maintain constant error relative to climatology. We expect that skill will decrease with averaging time.

a. Results for the coupled QG model

First we consider the dependence of background skill on slab-ocean depth and averaging time, holding the coupling strength fixed at $c = 0.25$, shown in Fig. 1. Each pixel is the skill of the background time-averaged state for a data assimilation experiment of length 100 assimilation cycles, area-averaged over the meridional center of the domain (the region of basic state meridional temperature gradient). We show skill for the surface temperature in the atmosphere; skill at the tropopause is nearly identical. The slab ocean depth d is represented by the ratio of the slab ocean heat capacity to the atmospheric heat capacity. Results show that for both the atmosphere and ocean, and for all depths of the slab ocean, skill decreases as the averaging time increases, consistent with prior expectation. There is a sharp drop of skill between 5 and 10 days, which we suspect corresponds to the model damping timescale of 8.6 days.

As slab ocean depth increases, skill in the ocean increases, as expected. In contrast, background skill for the atmosphere decreases with increasing slab-ocean depth, despite the fact that ocean temperature reconstruction is more skillful. We will revisit these conflicting results after reviewing those for the BB model.

Figure 2 shows the analogous experiment for fixed slab ocean depth ratio at $d = 4$, and varying the coupling parameter. For the atmosphere, skill increases slightly with increasing coupling coefficient. Skill in the ocean decreases as the coupling coefficient gets bigger. These results are consistent with expectations in the sense that the atmosphere is a source of noise for the ocean and the ocean is a source of thermal memory for the atmosphere.

In both Figs. 1 and 2 there is a striking difference between skill in the ocean and atmosphere. This is due to two factors. The first is simply the longer thermal inertia of the ocean. The process timescales in the ocean are each a factor of d longer than in the atmosphere, so persistence and predictability in the ocean should be longer. But even for $d=1$, when the ocean and atmosphere have the same heat capacity (not shown), the ocean has longer predictability than the atmosphere. One potential explanation is that since the ocean has no advection, it integrates over the faster dynamics in the atmosphere, which are dominated by advection, leading to higher skill at longer time averages.

b. Results for the stochastic energy-balance model

Before reporting the results from the BB model, we will compare its equilibrium statistical properties with those of the QG model, which it is meant to approximate. Cospectral analysis of the surface air and slab-ocean temperatures for the QG model are shown in Fig. 3, along with analytical spectra from the BB model. For the QG model, histograms of analyses are shown for each grid point in the center half of the domain in the y direction, where the basic state temperature gradient is nonzero. Analyses apply to the last 8000 days of an 8500 day integration. Ten-day blocks of un-normalized timeseries are averaged together, and then

cospectral analysis is carried out with a Hanning window of length 800 days using Matlab's **spectrum** function. Power spectra (P_a and P_o), cospectra (F_{ao}), and phase (ϕ) from the BB model are calculated from Eqs. (14) and (15) in Barsugli and Battisti (1998),

$$P_a(\sigma) = \frac{(d^2\sigma^2 + (c + \tau)^2)|N|^2}{((c + \tau)^2 - d\sigma^2 - bc) + \sigma^2(1 + d)^2(c + \tau)^2}, \quad (5)$$

$$P_o(\sigma) = \frac{c^2|N|^2}{((c + \tau)^2 - d\sigma^2 - bc) + \sigma^2(1 + d)^2(c + \tau)^2}, \quad (6)$$

$$F_{ao}(\sigma) = T_a T_o^* = \frac{c|N|^2(c + \tau + id\sigma)}{((c + \tau)^2 - d\sigma^2 - bc) + \sigma^2(1 + d)^2(c + \tau)^2}, \quad (7)$$

$$\phi = \tan^{-1} \frac{\text{Im}F_{ao}}{\text{Re}F_{ao}} = \frac{d\sigma}{c + \tau}, \quad (8)$$

where σ is the frequency, $(\cdot)^*$ indicates the complex conjugate, and $\alpha = bc$. Just one line is shown for the BB model, calculated with parameters $b = 0.5$ and $N = 5$, chosen by trial and error to correspond well the QG model spectra; other parameters are the same as those for the QG model.

As with the BB model, the spectra of the QG ocean and atmosphere increase toward lower frequencies; power in the system cannot increase indefinitely because of the damping terms. The cospectral power increases as frequency decreases in both the BB and QG models, and there is a low-frequency peak in the quadrature spectrum of both models. The atmosphere and ocean show high coherence at frequencies below $2\pi/100$ days⁻¹, which then degrades due to nonlinear effects at high frequencies. The phase relationship of the QG model follows very closely the BB phase at frequencies for which it is well defined. The close correspondence of the spectral characteristics of the two models lends confidence that the BB model provides a good approximation to the QG model for further analysis in a simpler framework.

The BB model data assimilation system discussed in section 2b provides the expected error statistics over an infinite number of experiments and ensemble members. The numerical

evaluation of Eq. (4), described more completely in the Appendix, begins with zero error and cycles until equilibrium is reached. Observations of both the air and slab ocean temperatures are assimilated with observational error taken to be 10% of the equilibrated error variance in the absence of assimilation. The evolution of the solution to equilibrium is shown in Fig. 4.

Skill as a function of averaging time and slab-ocean depth for fixed coupling strength is shown in Fig. 5 (compare to QG model results in Fig. 1). As in the QG experiments, skill decreases with increasing averaging time in both the atmosphere and ocean. Skill in the atmosphere decreases with increasing depth, and skill in the ocean increases with depth, which is also consistent with results from the QG model. A notable difference between the QG and BB model results is lower skill in the atmosphere of the BB model for all slab-ocean depths and averaging times.

Skill as a function of averaging time and coupling strength, for fixed slab-ocean depth, is shown in Fig. 6 (compare to QG model results in Fig. 2). Skill for air temperature decreases as coupling increases, which is the opposite of that found in the QG experiments. Skill for ocean temperature decreases as coupling increases, which is consistent with that found for the QG model. In summary, compared to the QG results, the BB system shows a similar response to varying slab-ocean depth, the same response to coupling for the ocean, but the opposite response to coupling in the atmosphere.

c. Decomposing error: accumulation of noise and initial condition

We can gain further understanding of the dependence of reconstruction skill on coupling strength and slab ocean depth from the error evolution equation (4) for the BB system. As discussed in section 2b, the error covariance evolution depends on two factors: the initial error at the start of an assimilation cycle and the accumulation of stochastic noise. We note that although the initial error depends on the noise error, observation error, and data assimilation system, the decomposition discussed here provides a useful perspective on the relative importance of initial error to accumulating noise in the forecast. Figure 7 shows the total error broken into these two terms as a function of slab-ocean depth. Assimilation is performed as for the previous assimilation experiments; the converged solution for the total error and its two component parts are plotted separately for the atmosphere and ocean. For the atmosphere, the fraction of the error variance attributable to initial error decreases slightly with increasing depth, while the part proportional to noise accumulation increases. The increase due to noise accumulation dominates, so that the total error increases with depth. For the ocean, the fraction of error due to noise decreases strongly with increasing slab-ocean depth, whereas the fraction due to initial error peaks at small depth and decreases gradually with depth so that it dominates the total error for large depth.

Results for sensitivity to the coupling strength are shown in Fig. 8. For the atmosphere noise error dominates over initial-condition error, as is the case for the depth experiments. For the ocean, initial-condition error dominates, as for the depth experiments. For the ocean, a notable difference from the depth experiments is that the noise error increases slowly with coupling, whereas it decreases sharply with increasing depth. A physical interpretation of

these sensitivity results is that deeper slab oceans are less sensitive to atmospheric noise due to increased thermal inertia, whereas stronger coupling increases the amount of noise introduced from the atmosphere, but this latter effect is weak compared to initial condition error.

4. Conclusions

The problem of reconstructing past climates from time-average observations has been explored within an idealized framework for midlatitude atmosphere-ocean interaction. A QG model coupled to a slab ocean was used to explore the hypotheses that skill in reconstructions will increase when (1) the depth of the slab ocean increases, and (2) the strength of the coupling increases. Results show that for increasing slab-ocean depth ocean skill increases as expected, but skill in the atmosphere does not. Skill increases slightly in the atmosphere for stronger coupling, but it decreases in the ocean. For both atmosphere and ocean, skill decreases with increasing observation averaging time.

The average freely-evolving behavior of the QG system was shown to correspond well to that of a simple two-variable linear stochastic model for midlatitude air-sea interaction (the BB system). Results for assimilation experiments for this system are similar to QG for sensitivity to slab-ocean depth, but not for coupling. An analytical expression for the BB error covariance forecast evolution helps explain these results. The atmosphere loses state-dependent skill faster than the ocean because the stochastic component of error accumulates more quickly than in the ocean. Moreover, the fraction of the total atmospheric forecast error variance due to stochastic noise increases with both slab-ocean depth and coupling

strength. That is, in the BB system, noise controls the solution more than initial-condition error. A physical interpretation of these results is that the ocean becomes thermally stiffer for increasing depth and coupling, so that noise “accumulates” in the atmosphere. For changes in coupling, responses are not consistent between the models. We speculate that advection of atmospheric anomalies combined with nonlinearities in the QG model cause this difference in behavior.

What do these results imply for climate reconstructions from data assimilation? Reconstructions from data assimilation are possible even when the “skill” of the forecast model at assimilation time, which was explored here, is no better than climatology. In this case, data assimilation can still be an improvement over statistical reconstruction, where climate covariances are a strong function of mean state, for example. The simple mixed-layer models considered here lack skill beyond a few months. Therefore, for the problem of paleoclimate data assimilation, a prerequisite is to establish that there is skill on longer time scales. This might happen with a model coupled to more slowly varying components such as the deep ocean or ice sheets. However, two more criteria must also be met: 1) the component’s fidelity to nature must be quantified, and 2) there should be a strong relationship between the slow component and the observed proxy.

Acknowledgments.

This research was sponsored by the National Science Foundation through grant 0902500, awarded to the University of Washington. The first author was also supported by fellowships from National Defense Science and Engineering Graduate fellowship program and

Achievement Rewards for College Scientists. The first author thanks Nils Napp for insightful conversations on stochastic calculus.

APPENDIX

Development and evaluation of error covariance.

Here we develop analytic expressions for error covariance evolution in the BB model, for both instantaneous, C_{total} , and time-averaged, $C_{average}$, cases. Note that the adjustment to the error covariance during the assimilation step does not require observation values, which is a convenient property of the Kalman filter. The calculation relies on stochastic calculus, an introduction to which is available in textbooks Øksendal (2003) and Gardiner (2004), as well as an article directed towards atmospheric scientists by Penland (2003).

a. Instantaneous error covariance

Rearranging the system of equations in the typical style of stochastic calculus, (3) becomes

$$d\vec{T}_t = \mathbf{A}\vec{T}dt + \mathbf{N}dB_t. \quad (\text{A1})$$

Using the integrating factor $e^{-\mathbf{A}t}$ yields the solution

$$\vec{T}(t) = e^{\mathbf{A}t}\vec{T}(0) + e^{\mathbf{A}t} \int_0^t e^{-\mathbf{A}s} \mathbf{N}dB_s. \quad (\text{A2})$$

We define the error of an ensemble member, or the ensemble mean, as the Euclidean distance from the true state, $\vec{T}_T(t)$: $\vec{\varepsilon}(t) = \vec{T}(t) - \vec{T}_T(t)$. Defining the expectation over an

infinite ensemble $\langle \cdot \rangle$ (where ensemble members are denoted by the random variable B_s), the ensemble error covariance is

$$C_{total}(t) = \left\langle (\bar{\varepsilon} - \langle \bar{\varepsilon} \rangle) (\bar{\varepsilon} - \langle \bar{\varepsilon} \rangle)^T \right\rangle = \langle \bar{\varepsilon}^* \bar{\varepsilon}^{*T} \rangle. \quad (\text{A3})$$

Deviations from the ensemble mean are denoted by $(\cdot)^*$, so $\bar{\varepsilon}^* \equiv \bar{\varepsilon} - \langle \bar{\varepsilon} \rangle = \vec{T} - \langle \vec{T} \rangle$.

Noting that the expectation over a random process vanishes ($\langle \int_0^t dB_s \rangle = 0$), the error of an ensemble member at time t is

$$\bar{\varepsilon}^*(t) = e^{At} \bar{\varepsilon}^*(0) + e^{At} \int_0^t e^{-As} \mathbf{N} dB_s. \quad (\text{A4})$$

Applying the expectation operators over ensembles and experiments to the squared error deviation $\bar{\varepsilon}^* \bar{\varepsilon}^{*T}$, all cross terms with only one term integrated over dB_s vanish. Noting that $\langle e^{At} \rangle = e^{At}$, the error covariance is,

$$\langle \bar{\varepsilon}^* \bar{\varepsilon}^{*T} \rangle = e^{At} \langle \bar{\varepsilon}^*(0) \bar{\varepsilon}^*(0)^T \rangle (e^{At})^T + \left\langle \left(e^{At} \int_0^t e^{-As} \mathbf{N} dB_s \right) \left(e^{At} \int_0^t e^{-As} \mathbf{N} dB_s \right)^T \right\rangle. \quad (\text{A5})$$

Distributing the last transpose, using Itô's isometry, and rearranging, the expected error covariance is,

$$\langle \bar{\varepsilon}^* \bar{\varepsilon}^{*T} \rangle = e^{At} \langle \bar{\varepsilon}^*(0) \bar{\varepsilon}^*(0)^T \rangle (e^{At})^T + \int_0^t e^{A(t-s)} \mathbf{N} \mathbf{N}^T (e^{A(t-s)})^T ds. \quad (\text{A6})$$

The two terms determine the error covariance evolution. The first is growth or decay of the initial error covariance, depending on the eigenvalues of \mathbf{A} . The second is the accumulation of noise, which increases the error covariance even when \mathbf{A} has only negative eigenvalues.

b. Error covariance of time-averaged states

The error of the time-averaged state is equal to the time-averaged error. Therefore, the error of a time-averaged state is given by

$$\bar{\varepsilon}^* = \frac{1}{L} \int_0^L \varepsilon^*(t) dt = \frac{1}{L} \int_0^L \left(e^{At} \varepsilon^*(0) + e^{At} \int_0^t e^{-As} \mathbf{N} dB_s \right) dt, \quad (\text{A7})$$

where $\bar{\cdot}$ denotes a time average and vector symbols are omitted for clarity.

Squaring the quantity above and applying the expectation operator, the cross-terms cancel as they did for the instantaneous error covariance, leaving

$$\begin{aligned} \langle \bar{\varepsilon}^* \bar{\varepsilon}^{*T} \rangle &= \frac{1}{L^2} \int_0^L e^{At} \varepsilon^*(0) dt \left(\int_0^L e^{At} \varepsilon^*(0) dt \right)^T \\ &+ \frac{1}{L^2} \left(\int_0^L \left(\int_0^t e^{A(t-s)} \mathbf{N} dB_s \right) dt \right) \left(\int_0^L \left(\int_0^t e^{A(t-s)} \mathbf{N} dB_s \right) dt \right)^T. \end{aligned} \quad (\text{A8})$$

Switching the order of integration and using Itô's isometry again yields

$$\begin{aligned} \langle \bar{\varepsilon}^* \bar{\varepsilon}^{*T} \rangle &= \frac{1}{L^2} \int_0^L e^{At} \varepsilon^*(0) dt \left(\int_0^L e^{At} \varepsilon^*(0) dt \right)^T \\ &+ \frac{1}{L^2} \int_0^L \left(\int_s^L e^{A(t-s)} \mathbf{N} dt \right) \left(\int_s^L e^{A(t-s)} \mathbf{N} dt \right)^T ds. \end{aligned} \quad (\text{A9})$$

The error covariance of time-averaged states evolves in an analogous fashion to the instantaneous states, depending on initial error and the accumulation of stochastic noise.

c. Evaluating the integrals

Since \mathbf{A} is linear and constant for the BB model, the evaluation of the covariance integrals is straightforward. The calculation will be shown only once, since all other terms can be solved in a similar manner.

The first term in the instantaneous error covariance equation (A6) can be evaluated directly. For the second term, we define $\mathbf{M}(t, s) = e^{\mathbf{A}(t-s)}$, so that the second term can be written as

$$\int_0^t \mathbf{M}(t, s) \mathbf{N} \mathbf{N}^T \mathbf{M}(t, s)^T ds = N^2 \begin{bmatrix} \int_0^t m_{11}^2 ds & \int_0^t m_{21} m_{11} ds \\ \int_0^t m_{21} m_{11} ds & \int_0^t m_{21}^2 ds \end{bmatrix}, \quad (\text{A10})$$

where the elements of \mathbf{M} are m_{ii} and depend on t and s . We calculate the elements of \mathbf{M} by doing an eigenvalue decomposition of \mathbf{A} , since if $\mathbf{A} = \mathbf{V} \mathbf{D} \mathbf{V}^{-1}$ then $e^{\mathbf{A}(t-s)} = \mathbf{V} e^{\mathbf{D}(t-s)} \mathbf{V}^{-1}$.

Then distributing and rearranging the elements of \mathbf{V} and \mathbf{D} yields

$$\mathbf{M}(t, s) = \frac{1}{\det(\mathbf{V})} \begin{bmatrix} v_{11} v_{22} e^{d_1(t-s)} - v_{12} v_{21} e^{d_2(t-s)} & -v_{11} v_{12} e^{d_1(t-s)} + v_{12} v_{11} e^{d_2(t-s)} \\ v_{21} v_{22} e^{d_1(t-s)} - v_{21} v_{22} e^{d_2(t-s)} & -v_{12} v_{21} e^{d_1(t-s)} + v_{22} v_{11} e^{d_2(t-s)} \end{bmatrix}. \quad (\text{A11})$$

The integral of each element of (A11) has three exponential terms: $e^{2d_1(t-s)}$, $e^{(d_1+d_2)(t-s)}$, and $e^{2d_2(t-s)}$, with all other quantities constant. This leaves the sum of many integrals of the form $\int_0^t e^{a(t-s)} ds$ for $a = 2d_1, d_1 + d_2$, and $2d_2$, which have solution

$$\int_0^t e^{a(t-s)} ds = \frac{1}{a} (e^{at} - 1). \quad (\text{A12})$$

Evaluating the error covariance of time-averaged states is similar to evaluating the instantaneous error covariances. The first term of (A9) is rewritten by distributing transposes and integrating (note that \mathbf{I} is the identity matrix and $(\cdot)^{-T}$ indicates an inverse and a transpose),

$$\frac{1}{L^2} \int_0^L e^{\mathbf{A}t} \varepsilon^*(0) dt \left(\int_0^L e^{\mathbf{A}t} \varepsilon(0) dt \right)^T = \frac{1}{L^2} \left(\int_0^L e^{\mathbf{A}t} dt \right) \varepsilon(0) \varepsilon^*(0)^T \left(\int_0^L (e^{\mathbf{A}t})^T dt \right) \quad (\text{A13})$$

$$= \frac{1}{L^2} \mathbf{A}^{-1} (e^{\mathbf{A}L} - \mathbf{I}) \varepsilon^*(0) \varepsilon^*(0)^T (e^{\mathbf{A}L} - \mathbf{I})^T \mathbf{A}^{-T}. \quad (\text{A14})$$

For the second term, we return to \mathbf{M} and its elements,

$$\begin{aligned} & \frac{1}{L^2} \int_0^L \left(\int_s^L \mathbf{M}(t, s) \mathbf{N} dt \right) \left(\int_s^L \mathbf{M}(t, s) \mathbf{N} dt \right)^T ds \\ &= \frac{N^2}{L^2} \int_0^L \begin{bmatrix} \left(\int_s^L m_{11}(t, s) dt \right)^2 & \int_s^L m_{11}(t, s) dt \int_s^L m_{21}(t, s) dt \\ \int_s^L m_{21}(t, s) dt \int_s^L m_{11}(t, s) dt & \left(\int_s^L m_{21}(t, s) dt \right)^2 \end{bmatrix} ds. \end{aligned} \quad (\text{A15})$$

As in the instantaneous case, each of the elements of this matrix is the product of integrals over exponential terms. Each of the exponential integral parts can be broken down into

$$\begin{aligned} & \int_0^L \left(\int_s^L e^{a(t-s)} dt \int_s^L e^{b(t-s)} dt \right) ds \\ &= \frac{1}{ab} \left(-\frac{1}{a+b} (1 - e^{(a+b)L}) + \frac{1}{a} (1 - e^{aL}) + \frac{1}{b} (1 - e^{bL}) + L \right). \end{aligned} \quad (\text{A16})$$

Matlab implementation allows calculation of the error covariance of quantities averaged over time L from an initial error covariance. An example integration of the system is shown in Fig. 4.

REFERENCES

- Anderson, J., T. Hoar, K. Raeder, H. Liu, N. Collins, R. Torn, and A. Avellano, 2009: The data assimilation research testbed: A community facility. *Bull. Amer. Meteor. Soc.*, **90** (9), 1283–1296.
- Anderson, J. L., 2001: An ensemble adjustment Kalman filter for data assimilation. *Mon. Wea. Rev.*, **129** (12), 2884–2903.
- Barsugli, J. J. and D. S. Battisti, 1998: The basic effects of atmosphere–ocean thermal coupling on midlatitude variability. *J. Atmos. Sci.*, **55** (4), 477–493.
- Boer, G. J., 2000: A study of atmosphere–ocean predictability on long time scales. *Climate Dyn.*, **16** (6), 469–477.
- Boer, G. J. and S. J. Lambert, 2008: Multi-model decadal potential predictability of precipitation and temperature. *Geophys. Res. Lett.*, **35** (5), L05706.
- Collins, M., 2002: Climate predictability on interannual to decadal time scales: the initial value problem. *Climate Dyn.*, **19** (8), 671–692.
- Davis, R., 1976: Predictability of sea surface temperature and sea level pressure anomalies over the North Pacific Ocean. *J. Phys. Oceanogr.*, **6** (3), 249–266.
- Deser, C., M. A. Alexander, and M. S. Timlin, 2003: Understanding the persistence of sea surface temperature anomalies in midlatitudes. *J. Climate*, **16** (1), 57–72.

- Dirren, S. and G. J. Hakim, 2005: Toward the assimilation of time-averaged observations. *Geophys. Res. Lett.*, **32** (4), L04804.
- Frankignoul, C. and K. Hasselmann, 1977: Stochastic climate models. Part II: Application to sea-surface temperature anomalies and thermocline variability. *Tellus*, **29** (4), 289–305.
- Gardiner, C. W., 2004: *Handbook Of Stochastic Methods: for Physics, Chemistry And The Natural Sciences*. 3rd ed., Springer, 415 pp.
- Gaspari, G. and S. E. Cohn, 1999: Construction of correlation functions in two and three dimensions. *Quart. J. Roy. Meteor. Soc.*, **125**, 723–757.
- Griffies, S. M. and K. Bryan, 1997: A predictability study of simulated North Atlantic multidecadal variability. *Climate Dyn.*, **13** (7-8), 459–487.
- Grotzner, A., M. Latif, A. Timmermann, and R. Voss, 1999: Interannual to decadal predictability in a coupled ocean-atmosphere general circulation model. *J. Climate*, **12** (8), 2607–2624.
- Hakim, G. J., 2000: Role of nonmodal growth and nonlinearity in cyclogenesis initial-value problems. *J. Atmos. Sci.*, **57** (17), 2951–2967.
- Hasselmann, K., 1976: Stochastic climate models Part I. Theory. *Tellus*, **28** (6), 473–485.
- Hoskins, B. and N. West, 1979: Baroclinic waves and frontogenesis. Part II: Uniform potential vorticity jet flows—Cold and warm fronts. *J. Atmos. Sci.*, **36**, 1663–1680.
- Huntley, H. S. and G. J. Hakim, 2009: Assimilation of time-averaged observations in a quasi-geostrophic atmospheric jet model. *Climate Dyn.*, 1–15.

- Jones, P. D., et al., 2009: High-resolution palaeoclimatology of the last millennium: A review of current status and future prospects. *Holocene*, **19** (1), 3–49.
- Koenigk, T. and U. Mikolajewicz, 2009: Seasonal to interannual climate predictability in mid and high northern latitudes in a global coupled model. *Climate Dyn.*, **32** (6), 783–798.
- Latif, M., 1998: Dynamics of interdecadal variability in coupled ocean-atmosphere models. *J. Climate*, **11** (4), 602–624.
- Latif, M., M. Collins, H. Pohlmann, and N. Keenlyside, 2006: A review of predictability studies of Atlantic sector climate on decadal time scales. *J. Climate*, **19** (23), 5971–5987.
- Mann, M. E., R. S. Bradley, and M. K. Hughes, 1999: Northern hemisphere temperatures during the past millennium: Inferences, uncertainties, and limitations. *Geophys. Res. Lett.*, **26** (6), 759–762.
- Meehl, G. A., et al., 2009: Decadal prediction: Can it be skillful? *Bull. Amer. Meteor. Soc.*, **90** (10), 1467–1485.
- Øksendal, B. K., 2003: *Stochastic Differential Equations: An Introduction With Applications*. 6th ed., Springer, 360 pp.
- Penland, C., 2003: A stochastic approach to nonlinear dynamics: A review (extended version of the article - "Noise out of chaos and why it won't go away"). *Bull. Amer. Meteor. Soc.*, **84** (7), 925–925.
- Pohlmann, H., M. Botzet, M. Latif, A. Roesch, M. Wild, and P. Tschuck, 2004: Estimating the decadal predictability of a coupled AOGCM. *J. Climate*, **17** (22), 4463–4472.

- Saravanan, R., G. Danabasoglu, S. C. Doney, and J. C. McWilliams, 2000: Decadal variability and predictability in the midlatitude oceanatmosphere system. *J. Climate*, **13** (6), 1073–1097.
- Saravanan, R. and J. C. McWilliams, 1998: Advective oceanatmosphere interaction: An analytical stochastic model with implications for decadal variability. *J. Climate*, **11** (2), 165–188.
- Schopf, P. S., 1985: Modeling tropical sea-surface temperature: Implications of various atmospheric responses. *Coupled ocean–atmosphere models*, J. C. J. Nihoul, Ed., Elsevier Science Publishers B.V., Elsevier Oceanography Series, Vol. 40, 727–734.
- Scott, R. B., 2003: Predictability of SST in an idealized, one-dimensional, coupled atmosphere–ocean climate model with stochastic forcing and advection. *J. Climate*, **16** (2), 323–335.

List of Tables

- 1 Values of parameters used as baseline in the BB and QG models. 28

TABLE 1. Values of parameters used as baseline in the BB and QG models.

	BB	QG	Description
d	20	20	Slab ocean heat capacity ratio (“depth”)
c	0.25	0.25	Coupling coefficient
τ	8.6	8.6 days	Damping timescale
b	0.5		Deterministic SST forcing
N	5		Noise forcing amplitude

List of Figures

- 1 Skill for QG data assimilation system (ensemble error variance at assimilation time normalized by control error variance) is shown, as a function of averaging time and slab ocean depth. Panel a is the atmosphere and panel b is the ocean. Coupling coefficient is $c = 0.25$. 31
- 2 As in figure 1, for varying coupling coefficient with slab ocean depth fixed at $d=4$. 32
- 3 Cospectral analysis of surface air and slab ocean temperature from QG model and the corresponding cospectra from BB model are shown. The power spectral density is shown in panel a for the surface air temperature and in panel c for the slab ocean temperature. The real part of their cospectrum is shown in panel b, and the imaginary part is shown in panel d. The coherence of the surface air temperature and slab ocean temperature for the QG model is shown in panel e; BB model coherence is always one because the model is linear. The phase lag of the slab ocean behind the surface air temperature is shown in panel f. A histogram for each frequency shows the relative frequency of spectral lines from QG model gridpoints. The contour interval is 0.1. The total power spectral density vertical integral for each frequency in each panel is one. 33

- 4 The error variance of time-averaged states for the BB data assimilation system is shown, with the atmosphere in the left panels (a, c, and e) and the ocean in the right panels (b, d, and f). The top panels (a and b) show the “Spinup” phase, where error grows asymptotically towards an equilibrium value without assimilating observations. The middle panels (c and d) show the “Control,” case, where error stays at the equilibrium value without assimilation. The bottom panels (e and f) show sawtooth plots (with both forecast and analysis error variance) for the “Assimilation” case, where observations with error variance of 1/10 of final spinup variance are assimilated. Model parameters are $c = 0.4$, $d = 20$, and an averaging time of 10 days. 34
- 5 Skill for the BB data assimilation system (error variance at assimilation time normalized by control error variance) is shown, as a function of averaging time and slab ocean depth, with the atmosphere in panel a and ocean in panel b. Coupling coefficient is fixed at $c = 0.25$. Compare with figure 1. 35
- 6 As in figure 5, with varying coupling coefficient, and slab ocean depth fixed at $d = 4$. Compare with figure 2. 36
- 7 BB forecast error variance as a function of slab ocean depth is shown, with the solid line showing the total and the broken and dash-dot lines showing initial and noise components of error. The atmosphere is shown in panel a and the ocean in panel b. Coupling coefficient is fixed at $c = 0.25$ and averaging time of 10 days. 37
- 8 As in figure 7, but as a function of coupling coefficient, with slab ocean depth fixed at $d = 20$. 38

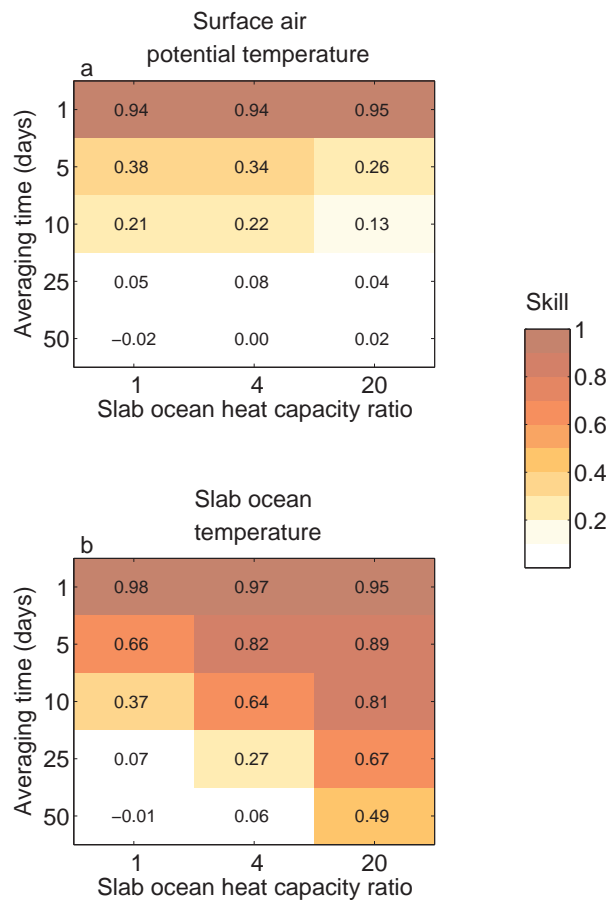


FIG. 1. Skill for QG data assimilation system (ensemble error variance at assimilation time normalized by control error variance) is shown, as a function of averaging time and slab ocean depth. Panel a is the atmosphere and panel b is the ocean. Coupling coefficient is $c = 0.25$.

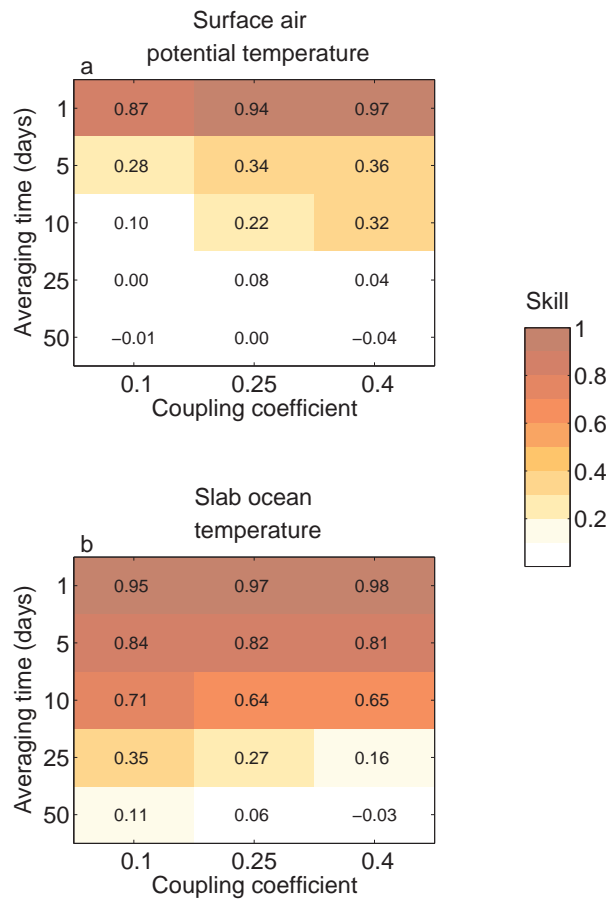


FIG. 2. As in figure 1, for varying coupling coefficient with slab ocean depth fixed at $d=4$.

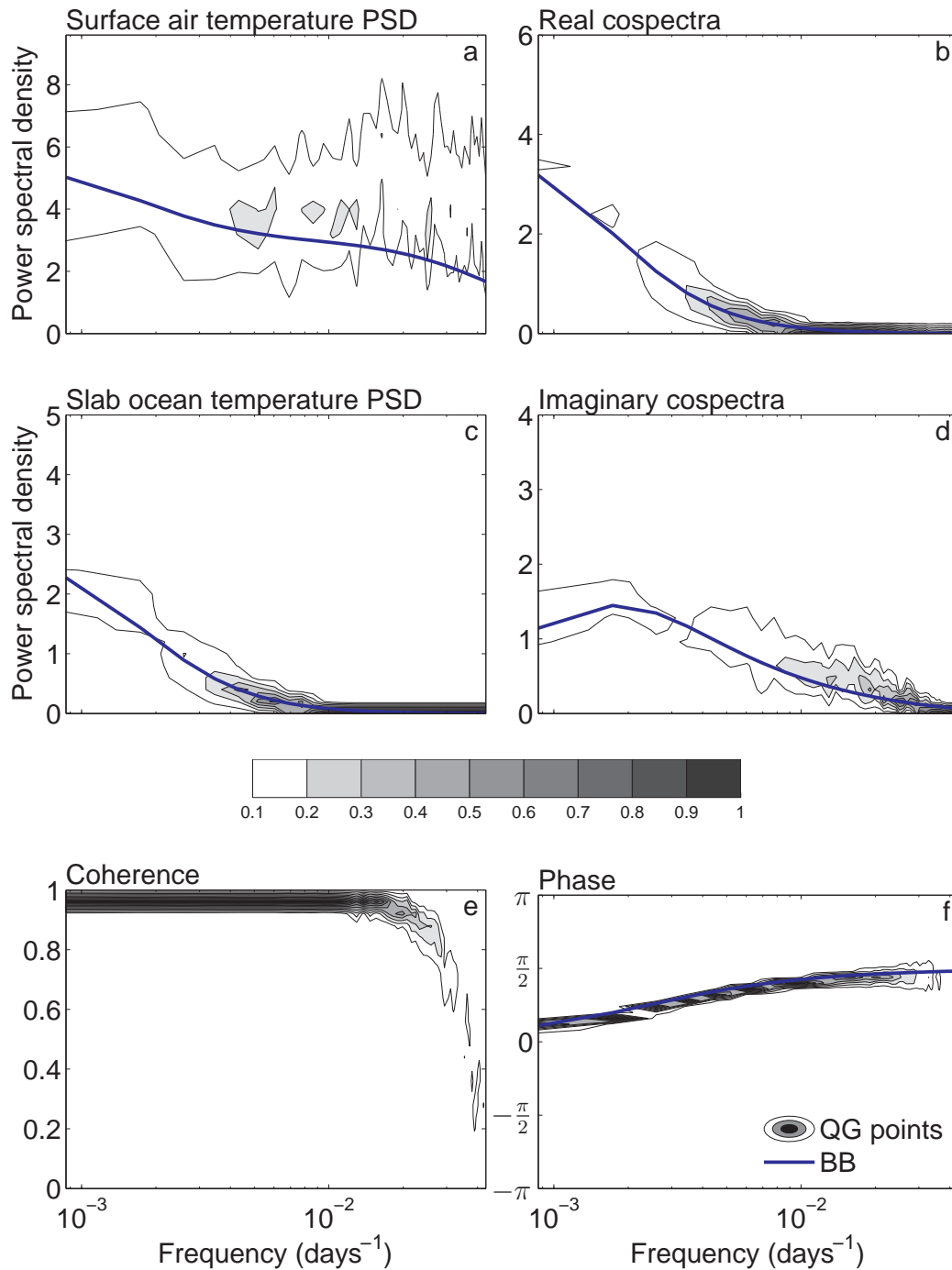


FIG. 3. Cospectral analysis of surface air and slab ocean temperature from QG model and the corresponding cospectra from BB model are shown. The power spectral density is shown in panel a for the surface air temperature and in panel c for the slab ocean temperature. The real part of their cospectrum is shown in panel b, and the imaginary part is shown in panel d. The coherence of the surface air temperature and slab ocean temperature for the QG model is shown in panel e; BB model coherence is always one because the model is linear. The phase lag of the slab ocean behind the surface air temperature is shown in panel f. A histogram for each frequency shows the relative frequency of spectral lines from QG model gridpoints. The contour interval is 0.1. The total power spectral density vertical integral for each frequency in each panel is one.

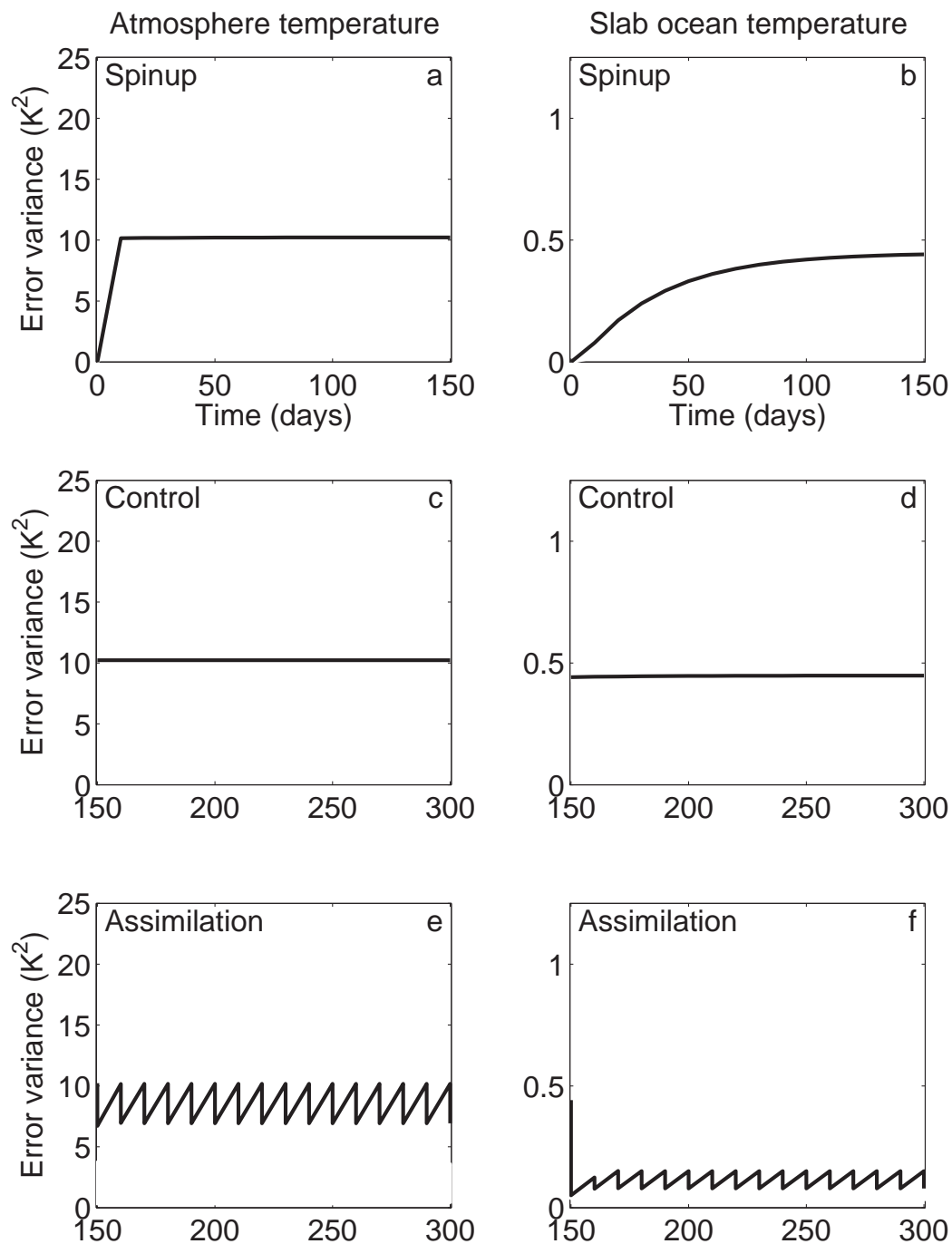


FIG. 4. The error variance of time-averaged states for the BB data assimilation system is shown, with the atmosphere in the left panels (a, c, and e) and the ocean in the right panels (b, d, and f). The top panels (a and b) show the “Spinup” phase, where error grows asymptotically towards an equilibrium value without assimilating observations. The middle panels (c and d) show the “Control,” case, where error stays at the equilibrium value without assimilation. The bottom panels (e and f) show sawtooth plots (with both forecast and analysis error variance) for the “Assimilation” case, where observations with error variance of 1/10 of final spinup variance are assimilated. Model parameters are $c = 0.4$, $d = 20$, and an averaging time of 10 days.

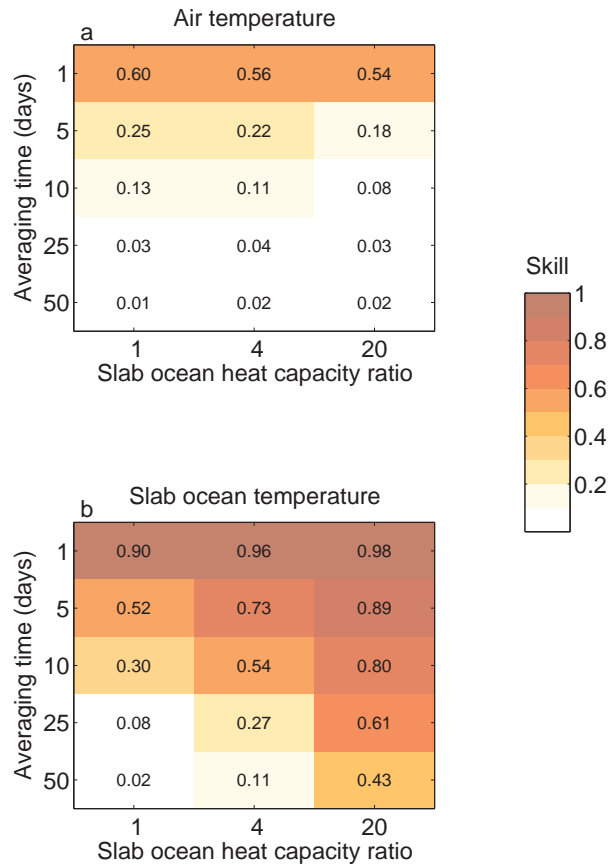


FIG. 5. Skill for the BB data assimilation system (error variance at assimilation time normalized by control error variance) is shown, as a function of averaging time and slab ocean depth, with the atmosphere in panel a and ocean in panel b. Coupling coefficient is fixed at $c = 0.25$. Compare with figure 1.

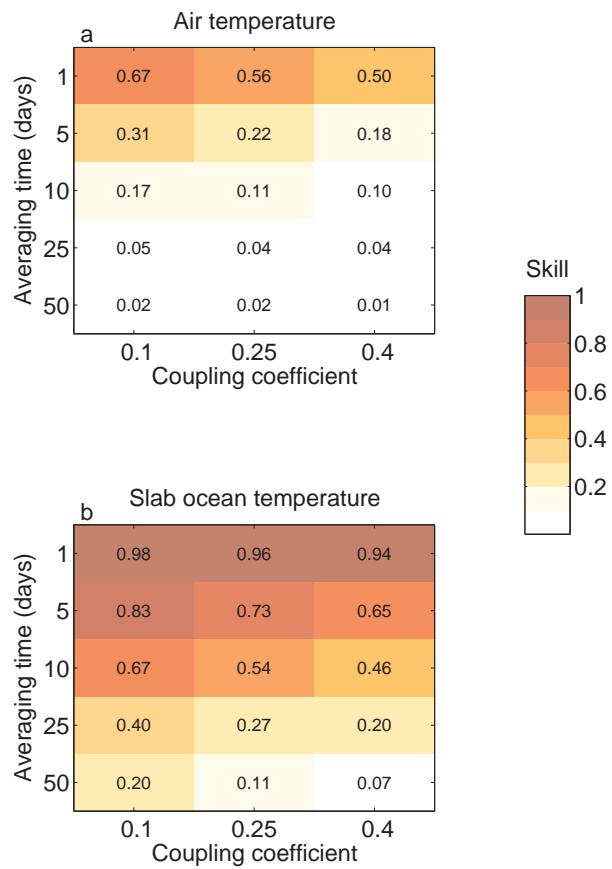


FIG. 6. As in figure 5, with varying coupling coefficient, and slab ocean depth fixed at $d = 4$. Compare with figure 2.

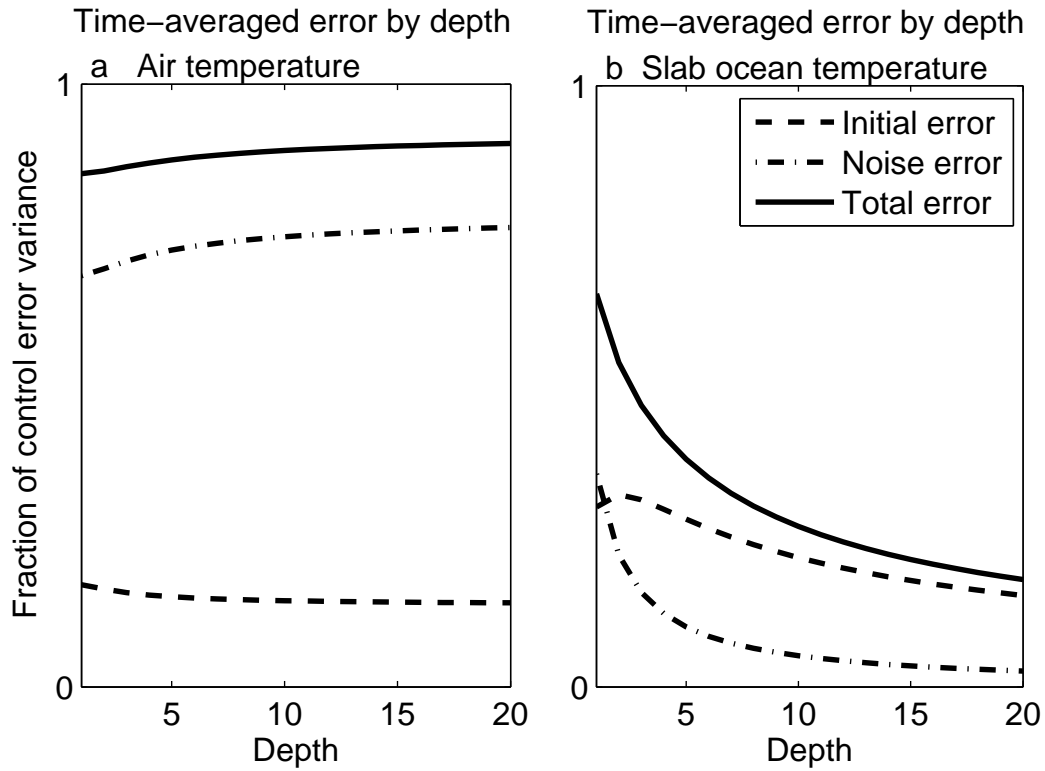


FIG. 7. BB forecast error variance as a function of slab ocean depth is shown, with the solid line showing the total and the broken and dash-dot lines showing initial and noise components of error. The atmosphere is shown in panel a and the ocean in panel b. Coupling coefficient is fixed at $c = 0.25$ and averaging time of 10 days.

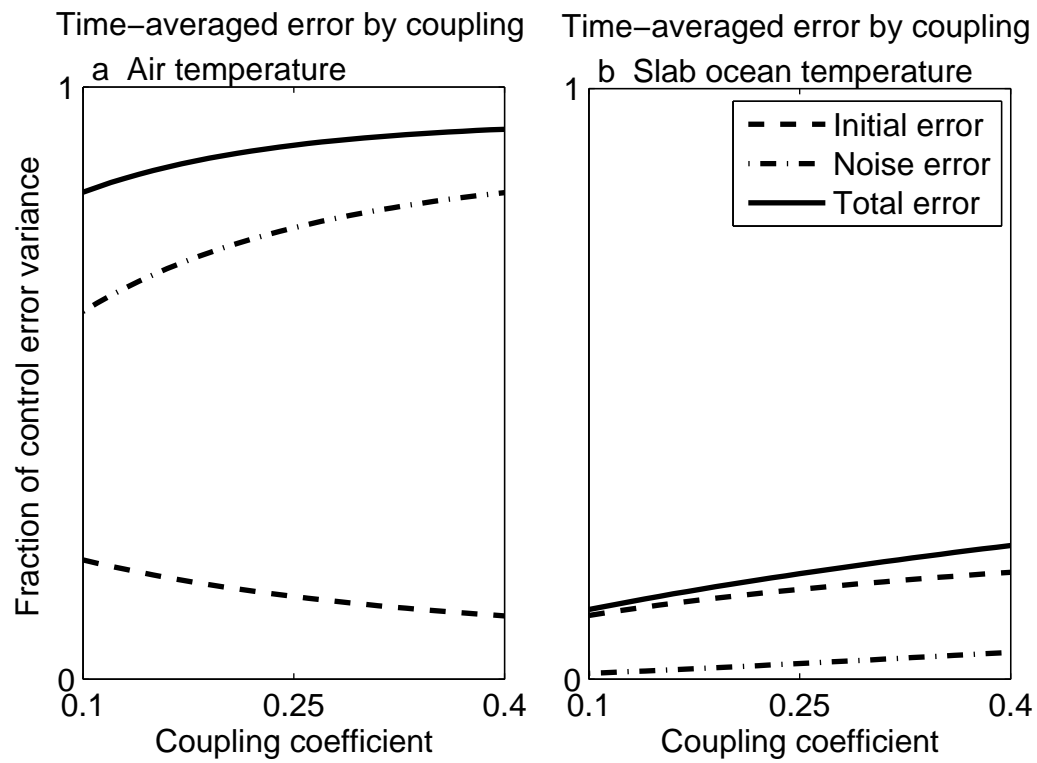


FIG. 8. As in figure 7, but as a function of coupling coefficient, with slab ocean depth fixed at $d = 20$.